Observation of Charge Transport in Single Titanium Dioxide Nanotubes by Micro-Photoluminescence Imaging and Spectroscopy

Candy C. Mercado, Fritz J. Knorr, and Jeanne L. McHale*

Materials Science and Engineering Program and Department of Chemistry, Washington State University, Pullman, Washington 99164-4630, United States

ABSTRACT We present the first report of photoluminescence spectra and images of single TiO_2 (anatase) nanotubes. In previous work using ensembles of conventional TiO_2 nanoparticles, we interpreted the broad photoluminescence (PL) spectrum to be a superposition of hole trap emission, peaking in the green, and broad red PL arising from electron traps. PL spectra of individual nanotubes in inert environment show a similar broad emission, with peaks at around 560−610 nm. The PL from single nanotubes differs from the more blue-shifted PL of ordered nanotube films. The intensity of PL is found to be larger for single nanotubes than for ordered arrays, as a result of competition from transport in the contiguous samples and from introduction of additional trap states when the nanotubes are dispersed. PL images of single nanotubes show the emission to be concentrated in the area of excitation, but the peaks in the red and green components of the PL are not spatially coincident. Remote PL, occurring away from the excitation point, is observed in the green (~510 nm), showing the possible contribution of charge transport to the observed PL. While the PL from ensembles of TiO_2 nanotubes is fairly insensitive to contacting media, exposure of single nanotubes to air and ethanol changes the shape and intensity of the PL spectrum. Our results point to a very different trap state distribution in TiO_2 nanotubes compared to that of conventional TiO_2 nanoparticles, which we attribute to differences in exposed crystal facets. In addition, separation of nanotubes introduces additional photoluminescent trap states and changes the character of the emission from excitonic in the array to trap-mediated in single nanotubes.

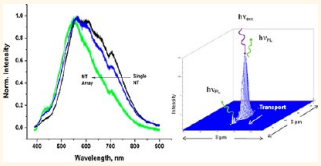

KEYWORDS: TiO_2 nanotubes · single nanoparticle spectroscopy · trap states · transport

Surface defects strongly influence macroscopic properties and device performance in applications of TiO_2 nanoparticles. For example, intra-band-gap states resulting from defects play an important role in carrier recombination and transport in TiO_2-based dye-sensitized solar cells (DSSCs).[1−4] While inefficient interparticle electron transfer hinders charge collection in conventional nanoporous TiO_2,[5] it was expected that the ordered structure of TiO_2 nanotube films would result in faster transport.[6] However, measurements showed that transport in nanotube-based devices is not significantly faster than that in films containing conventional TiO_2 nanoparticles,[7] although recombination rates are lower in the former.[8] It has been suggested that differences in trap state distributions result in more efficient charge collection in TiO_2 nanotubes than in conventional TiO_2 nanoparticles,[7,8] and that excitonic states limit transport in nanotubes.[9] Transport in nano-TiO_2 occurs by diffusion mediated by shallow traps, while deep traps promote deleterious recombination.[10−12] Additional factors that may influence transport are local electric fields,[13] solvent environment,[14] particle interconnectedness,[15] and, in the case of nanotubes, the morphology of the ordered films.[16] Trapping and detrapping events may be the major contributors to lower mobility in nano-TiO_2 compared to the bulk material,[11,13] and it is therefore of great interest to understand how trap states of conventional TiO_2 nanoparticles may differ from those of TiO_2 nanotubes.

We have previously used photoluminescence (PL) spectroscopy of nanocrystalline TiO_2 films to explore the dependence of trap state emission on contacting solvent,[17] surface treatment and crystalline phase,[18] sintering,[19] and nanoparticle morphology.[20] On the basis of these studies, we have formulated a model for the visible trap state emission of anatase TiO_2, which we assign to the radiative recombination of spatially isolated trapped electrons and holes with mobile carriers in the valence or conduction band, respectively. Recombination of mobile electrons with trapped holes results in emission that peaks in the green (~530 nm), while the recombination of trapped electrons

* Address correspondence to jmchale@wsu.edu.

Received for review May 30, 2012 and accepted July 24, 2012.

Published online July 24, 2012
10.1021/nn302392p

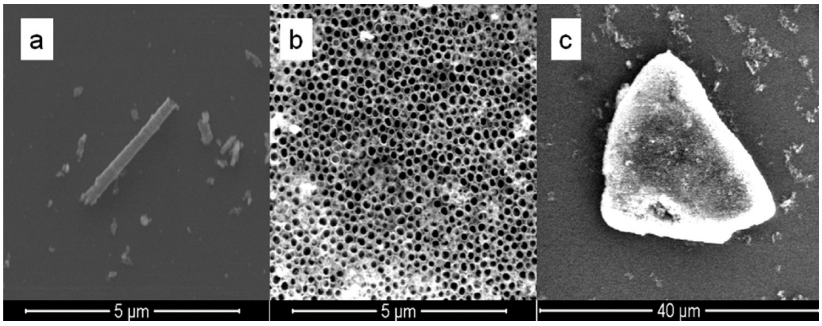

Figure 1. SEM images of dispersed TiO_2 nanotubes spin-coated onto a quartz coverslip: (a) single NT and fragments, (b) nanotube array fragment approximately 10 μm × 10 μm, (c) lower magnification image of this fragment.

with valence band holes leads to a broader PL spectrum with a peak in the red (~600 nm). We hypothesize, based on results summarized in ref 20, that trapped holes are isolated on the (101) surfaces of conventional anatase nanoparticles while electron traps associated with undercoordinated $Ti^{4+/3+}$ on the (001) planes are responsible for the PL that peaks in the red. In conventional TiO_2 nanoparticles (NPs), the (101) surfaces make up the majority of the surface, with the more reactive (001) surfaces contributing about 10%.[21] In the case of ordered anatase titanium dioxide nanotubes (NTs), the emission is centered at 550 nm and is much less intense and less responsive to environment than the PL of NP films.[20,22] Since radiative recombination of trapped and mobile carriers depends on their spatial overlap, the intensity of trap state PL diminishes when transport is faster. Thus the weaker intensity of PL from TiO_2 NTs compared to NPs could result from a lower density of intra-band-gap states and/or from improved transport. In addition, we have found[20] that the walls of the NTs expose (110) and (100) facets, which are not prevalent in conventional NPs. Hence different distributions of exposed surfaces could be tied to different trap state distributions and different PL spectra.

Hindering any study of surface trap states in nano-TiO_2 is the heterogeneity of the particles and their surfaces. Single nanoparticle luminescence addresses this problem by obtaining PL spectra of individual nanoparticles or small aggregates thereof. A few previous single nanoparticle PL studies of TiO_2 have been reported. Tachikawa *et al.* reported PL spectra and images of single nanowires of TiO_2—B[23] and of Eu^{3+}-doped TiO_2 nanoparticles,[24] while Jeon *et al.* reported PL blinking dynamics of single TiO_2 nanodisks.[25] In this work, we present the first report of PL spectra and images of individual TiO_2 nanotubes and address the nature of their trap states as compared to those of conventional TiO_2 nanoparticles as well as nanotube arrays.

RESULTS AND DISCUSSION

SEM Images. Figure 1 shows SEM images of the nanotubes. Ultrasonic dispersion of nanotube arrays resulted in single NTs and fragments shorter than the original thickness of the NT array (Figure 1a) and fragments of the NT array (Figure 1b,c). Figure 1b shows the top view of a fragment of the NT array revealing the perpendicular alignment of the tubes on the quartz substrate, while the single NT images shown below will be for NTs with their long axes parallel to the surface. The lengths of the single NTs analyzed were from 1 to 5 μm, while the original NT length in the ordered arrays was 10 μm. The nanotubes have external diameters ranging from 150 to 170 nm and wall thicknesses around 18 nm. In what follows, we will refer to arrays such as that shown in Figure 1b,c as "array fragments" to distinguish them from the contiguous NT arrays prepared on Ti substrate. TEM images of separated NTs, shown in Figure S1 of Supporting Information, reveal that the surfaces of the dispersed tubes are littered by broken fragments of nanotubes, mainly due to the TEM sample preparation where a drop of the suspension is allowed to dry on the copper grid. However, as will be shown below, the PL from the smaller fragments does not appear to be fundamentally different from that of more intact NTs.

Raman Spectra. As shown in Figure 2, Raman spectroscopy confirms that the TiO_2 NTs are in the anatase phase, in agreement with the XRD results shown in Figure S1 of Supporting Information. Figure 2 compares the Raman spectrum of an isolated NT (or perhaps a small bundle) to that of a fragment of the NT array and a cluster of anatase TiO_2 NPs. The relative intensities of the A_{1g} (399 cm^{-1}), B_{1g} (519 cm^{-1}), and E_g (639 cm^{-1}) peaks are similar for the single NT and NT array fragment, but the absolute intensities are, of course, smaller for the single NT. The relative intensities of these three peaks are different for nanotube and conventional nanoparticle samples owing to differences in nanoparticle morphology.

Photoluminescence Spectra. Figure 3 shows the micro-PL spectrum of a single NT (SNT) compared to that of a contiguous NT array (NTA) and a cluster of dispersed NPs as a function of excitation power. The corresponding (representative) SEM images of the three samples are also shown. In obtaining micro-PL spectra of films

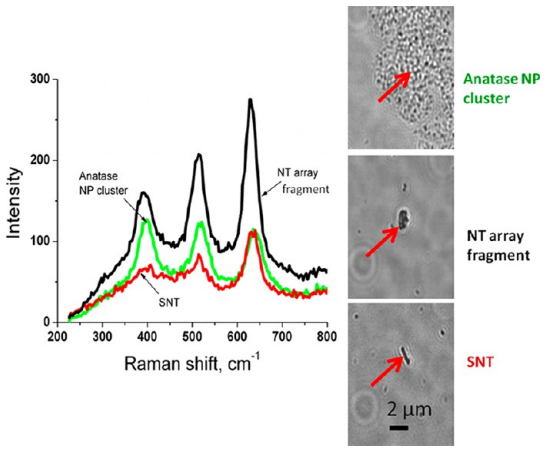

Figure 2. Raman scattering spectra excited at 413.1 nm of a NT array fragment, a single NT (SNT), and anatase NP clusters. Optical images are shown on the right.

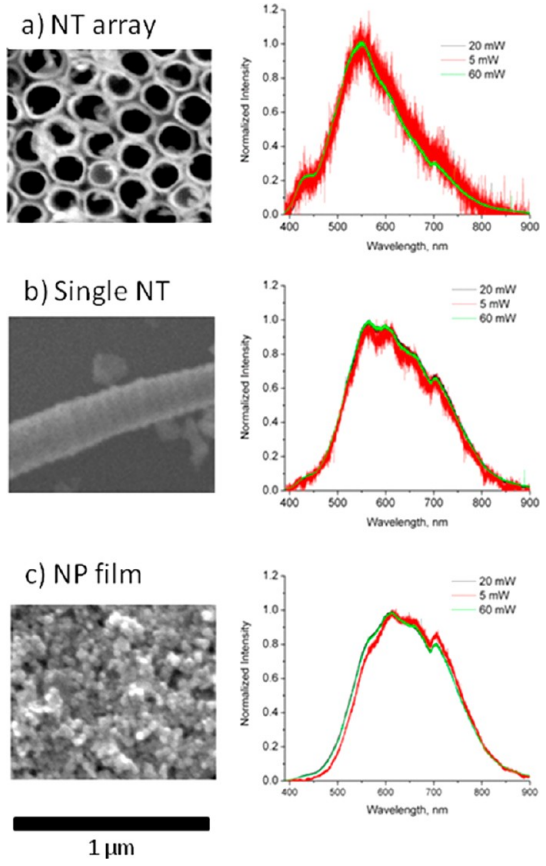

Figure 3. SEM images and normalized micro-PL spectra of (a) a contiguous NT array, (b) a single NT, and (c) a film of anatase NPs, as a function of laser power.

and isolated particles, the power density is of interest because, as shown in Supporting Information (Figure S2), higher powers can change the shape of the PL spectrum. For conventional anatase NPs, a blue-shifted spectrum at higher power densities results from increased contribution from the radiative recombination of mobile electrons with trapped holes. The similar normalized spectral line shapes in Figure 3 show that

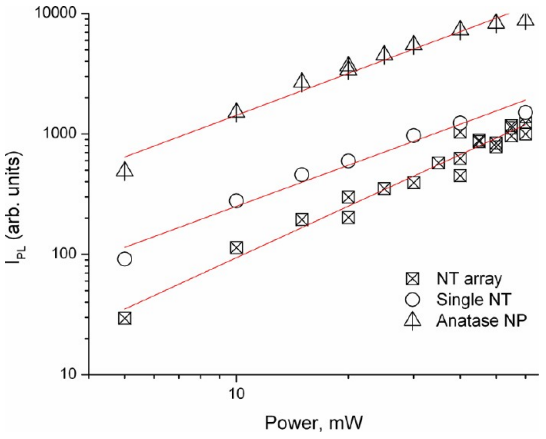

Figure 4. Dependence of peak PL intensity on incident laser power for an anatase NP film (triangles), a single NT (circle), and a contiguous NT array (black square). The red line is a least-squares fit.

the spectra are not being perturbed by high power densities of the microscope. The line shapes of the three different samples are clearly different. The micro-PL spectrum of a fragment of the NP film (Figure 3c) is identical to our previously reported spectra of both mesoporous[17,18] and dense[26] anatase NP films, while the emission spectrum of the NTA is narrower and blue-shifted relative to that of the NPs. The emission spectrum of the SNT, however, is intermediate between the two and shows enhanced emission in the red relative to the NTA. Though all three samples in Figure 3 show a broad range of emission wavelengths, both isolated and clustered nanotubes show PL spectra for which the peak is blue-shifted relative to the PL spectrum of NPs. In addition, there is a decreased width of the PL spectrum of the NT array compared to the spectrum of an isolated NT.

Figure 4 compares the peak PL intensity of single NTs, a contiguous NT array, and a NP film as a function of incident laser power. As previously reported,[20,22] the PL of the NTA is less intense than that of a NP film. However, it is significant that the PL intensity of the SNT is greater than that of a NTA. This is especially striking since the penetration depth of the incident light, about 0.5 μm based on the absorption coefficient at 350 nm from ref 27, is larger than the outer diameter of the NTs but smaller than the lengths of the ordered NTs. Thus the incident light excites a much greater sample volume in the case of the ordered array. This hints at the importance of transport in limiting the PL intensity. However, the electric field vector of the incident laser is oriented differently in the two samples, being coplanar with the long axis of the single NTs and perpendicular to the long axes of the ordered NT arrays. The polarization of the laser could select a different distribution of trap state emissions for NTs which are parallel *versus* perpendicular to the substrate. To check for this possibility, ensemble PL spectra of the as-prepared NT array were excited using a near-backscattering (~135°)

geometry and both vertically and horizontally polarized incident light. As shown in Figure S3 of Supporting Information, there is no difference in the PL spectra for these two experiments; thus, the difference in the spectra of single NTs and NT arrays is not a consequence of the different alignments of the tubes relative to the incident electric field vector. Alternatively, the interparticle connections in the NT arrays could passivate a subset of more red-emitting traps or permit interparticle transport that competes with the radiative recombination from these traps. The higher PL intensity of a single NT compared to a NT array, while surprising at first, may be a consequence of the higher probability of radiative recombination of trapped and mobile carriers when the nascent electron–hole pairs are confined to a smaller sample volume. In addition, the enhanced emission in smaller nanoparticles could result from diminished competition from nonradiative relaxation channels since the rate of PL quenching by electron or energy transfer decreases in confined geometries.[28]

Closer examination of the slopes of the plots in Figure 4 provides more insight into the nature of the emission in the different samples. In general, the intensity of photoluminescence I_{PL} is proportional to P^k, where P is the incident power and k is an exponent that can reveal the nature of the radiative recombination.[29] For the case of single NTs and conventional NPs, slopes close to unity ($k = 1.15 \pm 0.7$ for NPs and 1.13 ± 0.9 for the SNT) were observed in the log–log plots of Figure 4, decreasing slightly at higher powers. This behavior is consistent with recombination of mobile and trapped carriers, in accord with our previous model for the green and red PL components of conventional anatase NPs. For the contiguous NT array, however, we find $k = 1.42 \pm 0.06$. As discussed in ref 29, this is suggestive of a donor- or acceptor-bound excitonic transition. As will be considered further below, this indicates that separation of NTs changes the nature of their luminescent trap states.

Further consideration of the role of sample size is given in Figure 5, which reveals a weak trend toward decreased intensity of emission with increase in NT length. We interpret this to result from increasing competition from nonradiative recombination in longer NTs. The geminate electron hole pairs created in the illuminated volume diffuse away from the laser spot at different rates owing to different electron and hole mobilities.[30] Smaller particle sizes increase the chance that trapped and mobile carriers will overlap spatially and undergo radiative recombination. The scattered nature of the data in Figure 5 might result from our inability to distinguish bundles of NTs from single NTs in optical microscopy; hence there may be intensity variations that result from probing different numbers of NTs.

Figure 6 shows PL images of dispersed NTs under epi-illumination and with various filters. The images

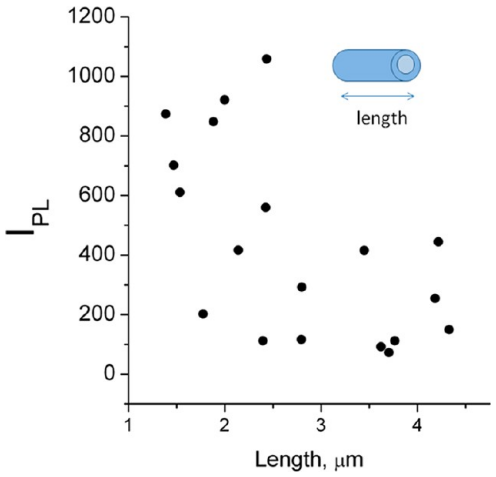

Figure 5. Peak intensity of single NT PL as a function of NT length.

obtained with the 510 nm band-pass filter are brighter than those obtained with longer wavelength light. The corresponding line profiles show that bright and dark areas of the NT are similar for the 510 nm filtered PL and unfiltered PL images. The PL intensity is distributed along the entire length of the tube, and there is no evidence that PL at green and red wavelengths emanates from different regions of the NT. Additional epi-illumination images of dispersed NTs and their corresponding SEM and optical images are shown in Figure S4.

Figure 7 shows the correlated PL and SEM images of a single NT and a NT array fragment, along with the PL spectra obtained from the same illuminated region. As in Figure 3, the emission spectrum of the SNT shows more intensity in the red than that of the ordered array. Good correlation between the optical images (shown as insets to the PL images) and SEM images is observed showing the ability to locate the same structure in both experiments.

Figure 8 demonstrates the interesting observation of satellite emission. Using either the 385 nm long-pass or the 510 nm band-pass filter to determine the PL image, a satellite luminescence is observed near one end of the ~4 μm nanotube. The satellite is not observed using the red long-pass filter. This behavior is similar to that observed in nanowires of TiO_2–B,[23] although the remote emission that was observed in that study was red (~600 nm). It is tempting to interpret the remote PL of NTs using our previously developed model for the trap state emission of conventional NPs,[20] where the emission peaking in the green is associated with mobile electrons recombining with hole traps on (101) exposed planes. However, (101) planes do not appear to make up a large portion of the NT surface.[20] Alternatively, we considered that the satellite emission results from waveguiding, as has been observed for example in ZnO[31] and TiO_2[23] nanowires. However, the wall thicknesses of our NTs, less

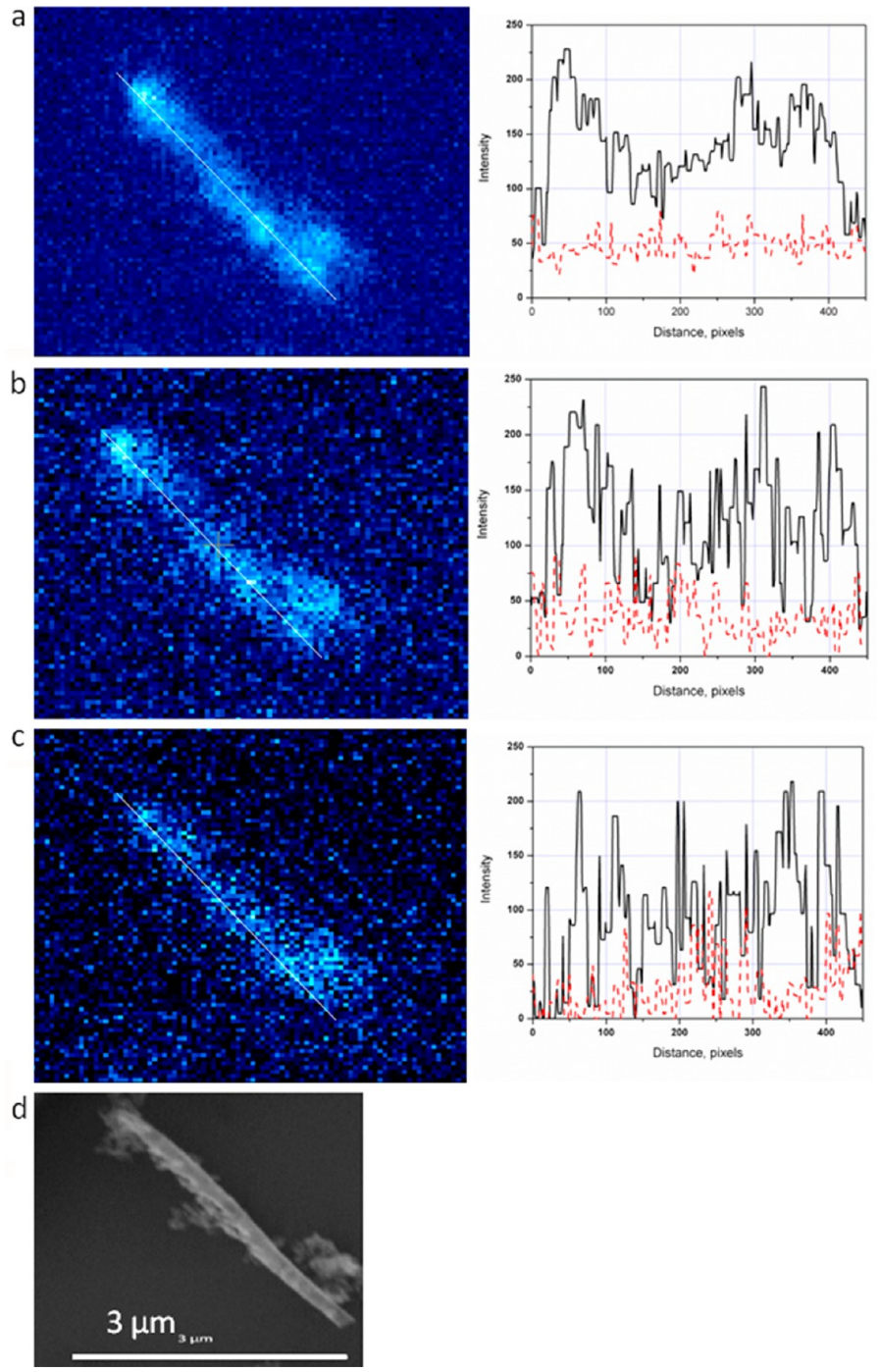

Figure 6. Photoluminescence of a SNT under epi-illumination with 20 mW of 350.7 nm laser (a) without a filter, (b) with the 510 nm band-pass filter, (c) with the 610 nm long-pass filter, (d) SEM image of the same area. The corresponding line scans on the right show the intensity along the white line in the PL image (black lines) compared to the background (red dotted lines).

than 20 nm, are much smaller than the dimensions of the nanowires used in refs 23 and 31. It is likely that diffraction effects would limit the ability of our NTs to confine visible light, and it is therefore reasonable to assign the remote emission to carrier transport. In this picture, mobile carriers formed in the illuminated region diffuse and recombine with pre-existing trapped charges at remote locations.

Figure 9 shows the PL images obtained from a pair of crossed NTs excited at four different positions. The presence of remote luminescent spots can be seen when illuminated in regions 2 to 4, revealing weak but observable emission from the shorter nanotube when the longer one is illuminated. On the contrary, excitation of the shorter tube (at region 1 in Figure 9) gave a completely dark longer tube. Excitation of the longer NT results in remote emission near the end of the tube.

Figure 10 shows the effect of air and ethanol on the PL spectrum of a single NT. We have previously

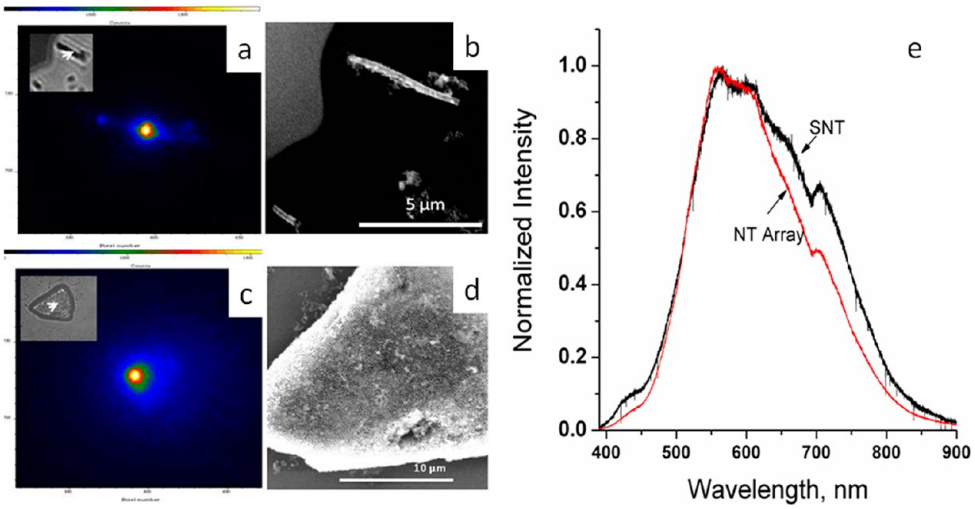

Figure 7. False color PL images of (a) a single NT and (c) a NT array fragment, with their corresponding SEM images in (b) and (d). The PL images were recorded with a 385 nm long-pass filter, and the optical image is shown as an inset. (e) PL spectra from the same single nanotube (SNT) and NT array samples.

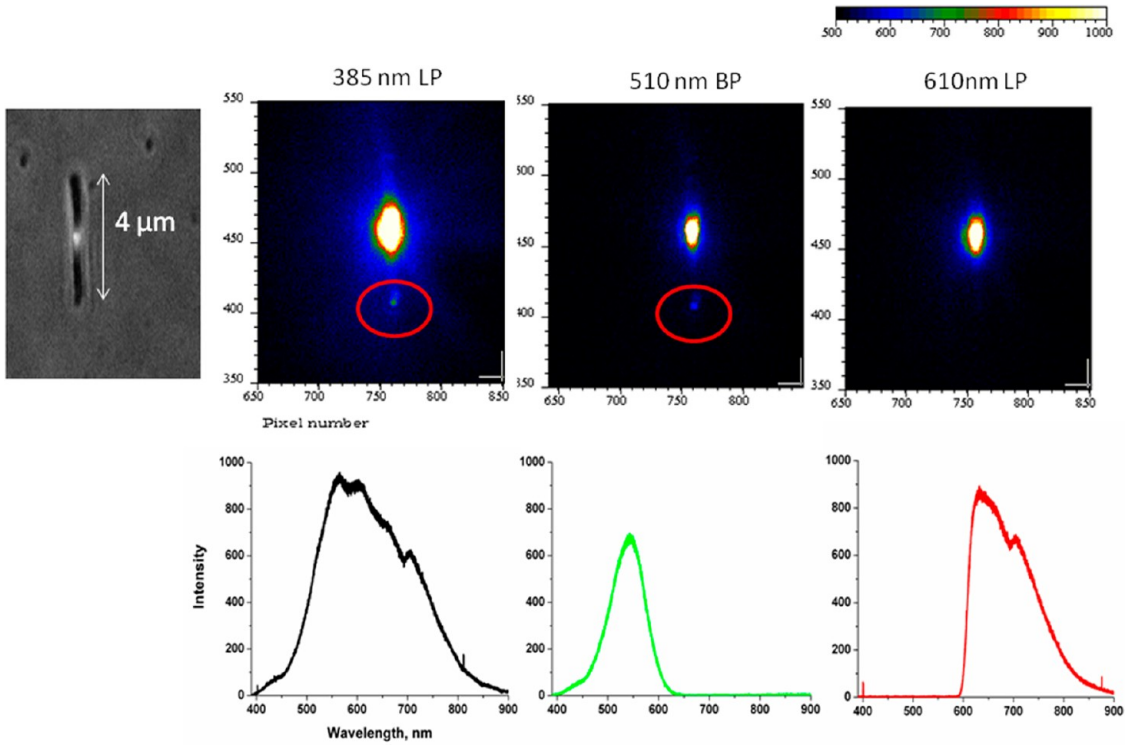

Figure 8. Optical image (top left) and corresponding PL images (top) and spectra (bottom) taken with 385 nm long-pass filter, 510 nm band-pass filter, and 610 nm long-pass filter. The red circle indicates the satellite emission observed with the first two filters.

shown[17] that, for conventional anatase NPs, air almost completely quenches the PL owing to electron scavenging, and ethanol acting as a scavenger of valence band holes[32] quenches the red emission from electron traps. In addition, we found that the PL of contiguous NT films is less dependent on environment than that of mesoporous anatase films, showing very little PL quenching when exposed to air.[20,22] As shown in Figure 10, the PL of single NTs also has a very different dependence on air and ethanol (EtOH) compared to the PL of bulk NP samples. In the SNT, air quenches the emission slightly on the red side. EtOH also quenches the emission on the red side of the spectrum but in addition causes an overall decrease in the emission intensity. In contrast, ethanol causes an increase in the intensity and a larger blue shift in the emission of anatase NPs, which we have attributed to a current doubling mechanism.[20,33,34] The data of Figure 10

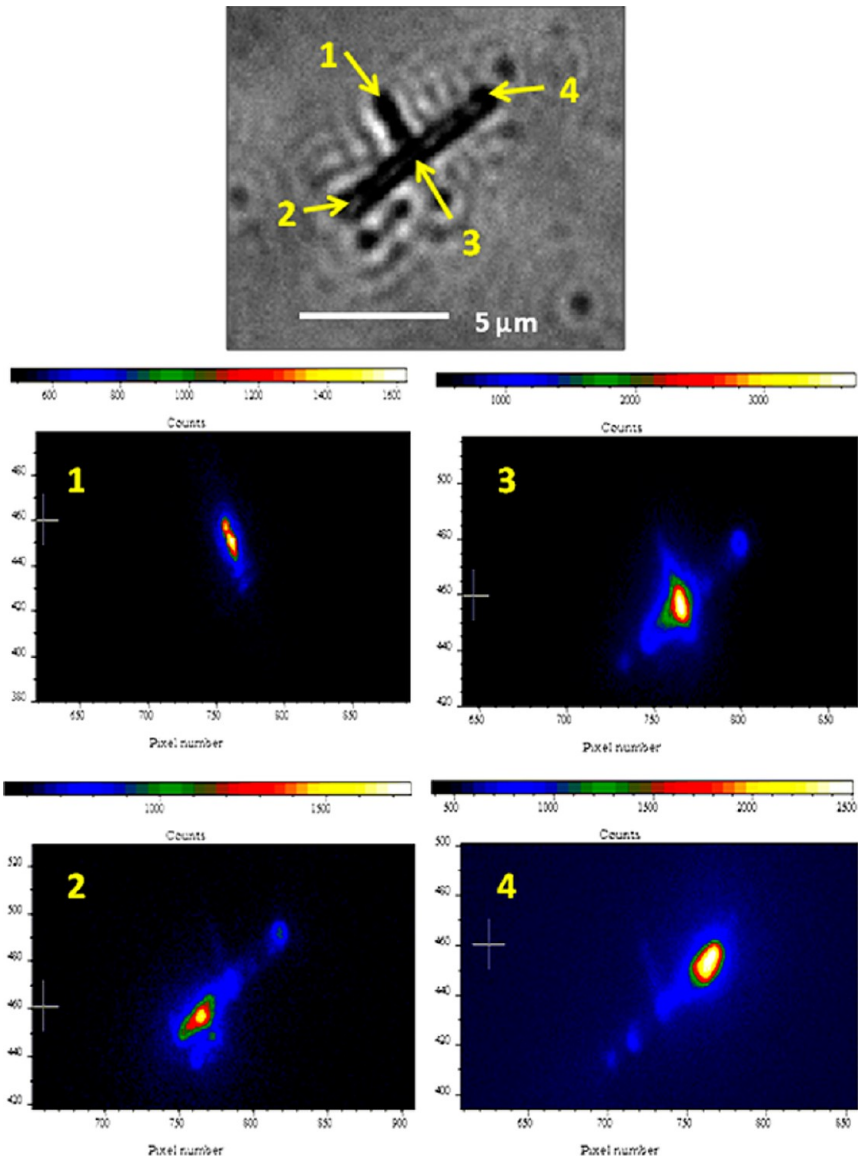

Figure 9. Optical image (top center) of a pair of crossed nanotubes and PL images (1 through 4) obtained upon excitation at the indicated positions. Recorded with a 385 nm long-pass filter.

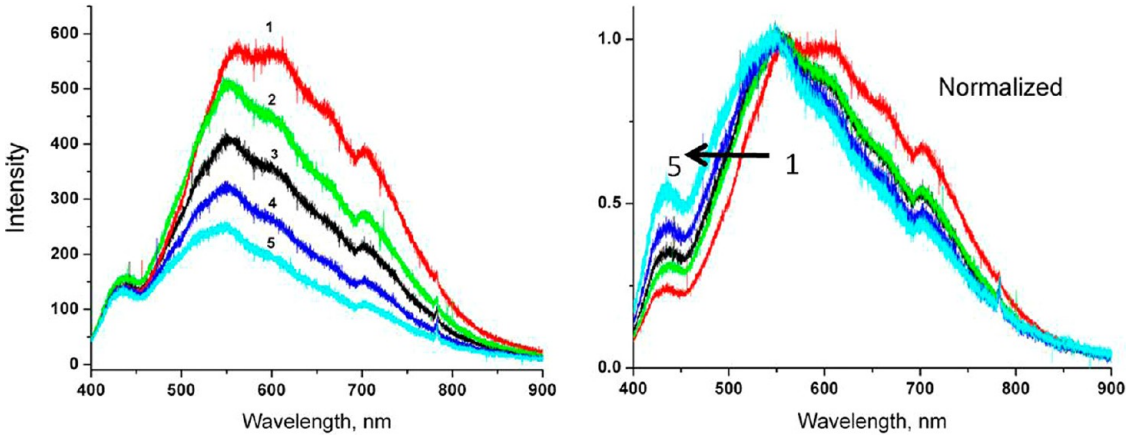

Figure 10. PL spectrum of a single nanotube (1) in Ar, (2) after 1 h in air, (3) immediately after introducing ethanol vapor, (4) after 30 min exposure to ethanol vapor, and (5) in liquid ethanol.

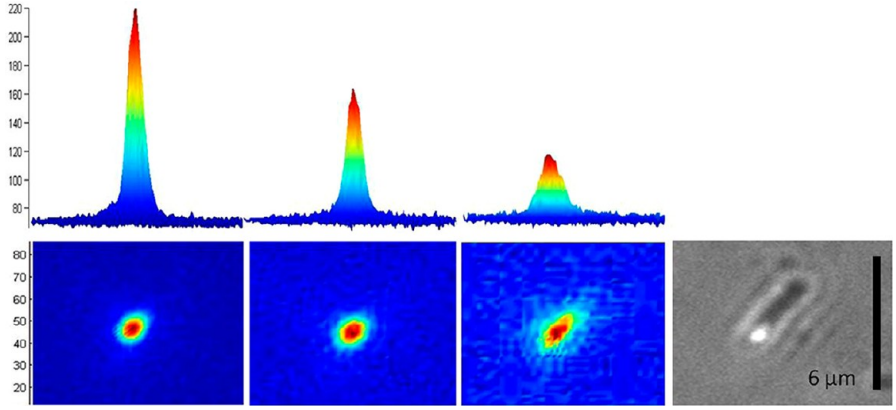

Figure 11. Intensity (top) and spatial distribution (bottom) of emission (from left) in argon, after 5 min in air, and after 12 h in air. The right-most image is the 100× optical image of the excited area with microscope illumination.

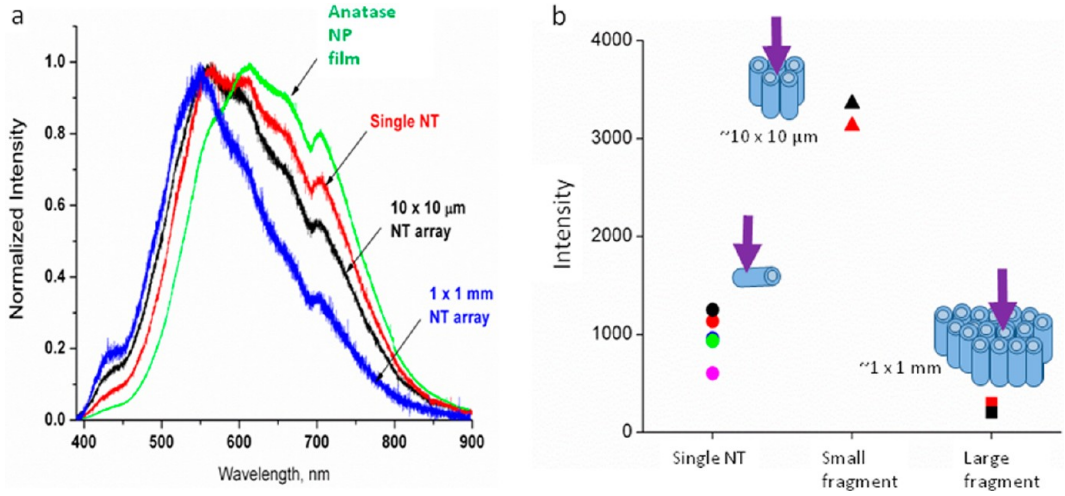

Figure 12. (a) Normalized PL spectra of different samples showing the diminished intensity of red PL for single NTs and NT arrays. (b) Characteristic PL intensity of single NTs compared to that of various sizes of NT array fragments.

suggest that the assignment of the red and green regions of the NT PL is different from that of NPs.

Figure 11 provides further insight into the effect of air on the PL. As shown there, the spatial distribution of the PL in argon is a symmetric Gaussian peak while prolonged exposure to air resulted in a PL image that is elongated to follow the dimension of the nanotube and decreased in intensity. Evidence suggests that O_2 adsorbs on oxygen vacancies in rutile and anatase.[26,34] In conventional anatase NPs, green emission appears to be associated with hole traps (*i.e.*, deep electron traps) from oxygen vacancies.[20] The results in Figure 11 hint at the role of oxygen vacancies in the NT emission and in impeding transport. Prolonged exposure to air could heal these vacancies, improving transport and resulting in a PL image which extends along the length of the NT.

Surprisingly large intensities are observed for the PL of single TiO_2 nanotubes, considering the weak PL of their contiguous ordered arrays. At the same time, emission on the red side of the PL spectrum of single NTs is apparently quenched in the ordered arrays, more so as the size of the fragment increases, as shown in Figure 12. These results suggest that there is significant charge transport perpendicular to the long axis of the tubes in the ordered arrays. The diminished red-edge PL in the ordered arrays could result from passivation of traps residing along the tube walls when the tubes are interconnected. The power dependence data of Figure 4 indicate a bound excitonic component to the PL of the NT array, consistent with conclusions of ref 9, that is absent in the separated NTs. Both oxygen and EtOH are capable of quenching the red edge of the single NT PL spectrum (Figure 10), and both are known to bind to oxygen vacancies. Differences between the PL of SNTs and NT arrays (NTAs) can be understood if we hypothesize that oxygen vacancy defects or other trap states are more numerous or more accessible in SNTs than in NTAs. It is reasonable to suppose that a larger number of trap states in SNTs than NTAs is responsible for the change in PL from a trap-assisted excitonic recombination in the array to recombination

of trapped and mobile carriers in the individual NT, in agreement with the power dependence of Figure 4. The excitonic character of the NTA PL is consistent with observed[20,22] weaker dependence of the spectrum on electron and hole scavenging environments compared to SNTs and NP films.

Our results suggest that both TiO_2 SNTs and NTAs have an entirely different distribution of emissive traps compared to that of conventional TiO_2 NPs. (An exception to this is the narrow peak at about 700 nm that is present in all anatase nanostructures and is likely assigned to electrons trapped at undercoordinated Ti sites.) Conventional TiO_2 NPs are well-known to have surfaces dominated by lower energy (101) facets, where hole traps associated with oxygen vacancies are located, while electron traps associated with undercoordinated Ti atoms prevail on the minority (001) surfaces.[20] TiO_2 NTs, on the other hand, exhibit growth along the [001] direction; therefore, not surprisingly, their walls expose (100) and (110) facets, which are not common in conventional NPs.[20] Thus the model of trap state emission we developed previously for conventional NPs, and for nanosheets exposing a lot of (001) surfaces, is not applicable to NTs. For example, PL quenching by oxygen may require a sufficient number of O_2 binding sites, which are known to be found on anatase (101). The presence of this surface also appears to be tied to the current-doubling mechanism that makes PL of conventional NP films increase in intensity in the presence of ethanol, a phenomenon which is not observed in the PL of NTs. We note that the effects of both ethanol and air on SNT PL is very similar to their effects on the PL of TiO_2 nanosheets with predominately (001) texture. We suggest the strong effects of ethanol and air on the PL of conventional anatase NPs depend on their ability to bind at oxygen vacancies on the (101) surfaces. In the intact NT films, the surfaces of the NTs may be unable to bind O_2 and thus no quenching is seen in air.[20]

CONCLUSION

Photoluminescence spectroscopy and imaging of single TiO_2 nanotubes permit the observation of carrier transport and radiative recombination of mobile and trapped charges. The emission spectrum of a single nanotube revealed more intensity on the red side of the spectrum compared to the spectra of ordered nanotube arrays. The power dependence of the PL from single NTs and NT arrays suggests that separation of the NTs changes the nature of the PL from that of a bound exciton to that of recombination of trapped and mobile carriers. We speculate that individual NTs possess more surface defects than NTs in contiguous arrays, and that these defects contribute to the red-edge PL that is seen in SNTs but not in NTAs. Supporting this, we found that emission at red wavelengths can be quenched by both oxygen and ethanol, presumed to bind at oxygen vacancies, when the nanotubes are separated. Decreased lateral charge transport in separated NTs, along with increased trap state activity, explains why the PL is orders of magnitude brighter in SNTs than in NTAs. The excitonic character of the NTA PL and scarcity of binding sites explain our previously puzzling observation[22] that this PL is fairly insensitive to the presence of electron and hole scavengers. Though the exposed surfaces and trap state distributions of SNTs differ from those of conventional NPs, the present results suggest a similar assignment of the PL at green and red wavelengths to recombination of trapped holes and trapped electrons, respectively, with oppositely charged mobile carriers. Given the longer diffusion length of electrons compared to holes in anatase,[35,36] the observation of remote PL in SNTs at green, not red, wavelengths could be explained if PL in the green derives from recombination of mobile electrons with neutral acceptors, such as hole traps. Ethanol, which scavenges valence band holes but not trapped holes,[37] cannot quench this green PL but does diminish the PL on the red edge, which is then attributed to recombination of trapped electrons with valence band holes. While this model is similar to that for conventional anatase NPs, the shapes of the PL of NPs and NTs differ because the surface traps are situated on different facets.

Assuming the emission in the NT array is that of a donor-bound exciton, the energy of the emission is $h\nu = E_g - E_x - E_D$, where E_D is the donor binding energy, E_x the exciton binding energy, and E_g = 3.2 eV is the band gap. The recombination of trapped electrons with valence band holes, on the other hand (*e.g.*, the "red PL" of conventional anatase NPs), occurs at $h\nu = E_g - E_D$. Similar equations can be written to compare acceptor-bound excitonic transitions to the green PL of anatase NPs (the recombination of mobile electrons with trapped holes), by replacing E_D by the acceptor binding energy E_A. Thus the large Stokes shift and breadth of the PL in either case are a consequence of the range and depth of electron (or hole) traps, in addition to probable phonon progressions. In the model proposed here, suggested by the difference in the power dependence of the PL of SNTs and NTAs, the introduction of additional trap states, which could be either donors or acceptors, when the nanotubes are dispersed, changes the nature of the PL from a donor- or acceptor-bound exciton, in the NTA, to radiative recombination of trapped and mobile carriers, in the SNT. The excitonic character of the PL of the NTA, along with the lower density of active traps that can bind air and ethanol, explains the very weak dependence of the PL on the presence of electron and hole scavengers. Many TiO_2 samples, including amorphous nanoparticles, show a narrow emission at ~420 nm that is insensitive to surface treatment, which we assign to a self-trapped exciton.[17,18,38] Thus the binding energy

E_x of about 0.25 eV contributes to the Stokes shift of the PL from NTAs.

The difference in the nature of the photoluminescence in individual NTs *versus* NT arrays might appear to obscure the question of the influence of lateral carrier transport on the intensity of PL. However, the orders-of-magnitude increase in PL intensity in the SNTs appears difficult to account for by a mere increase in trap density. Consistent with the conclusions of ref 16, we invoke lateral carrier transport between connecting NTs in the array, which serves to quench the PL from recombination of free and trapped carriers, in the contiguous NT arrays.

Returning to one of the original questions we hoped to address by single nanoparticle spectroscopy, our results show that the breadth of the PL spectrum is *not* an ensemble effect since different SNTs give identical spectral shapes. Broadening by phonon modes is one example of a homogeneous broadening effect that could account for the observed emission spectral widths. Further, the epi-illumination images show luminescent traps to be dispersed along the entire length of the NT, with no evidence for spatial separation of traps emitting at different wavelengths. Future work will be aimed at determining the molecular nature of these traps.

EXPERIMENTAL SECTION

Titanium foils (99.7% from Aldrich) were anodized at 50 V in 3% NH_4F, 2% water, and ethylene glycol electrolyte for 48 h.[39] The resulting TiO_2 nanotube films were then washed with ultrapure water and sintered in air at 450 °C for 3 h, then ultrasonically dispersed in ethanol for 30 min and spin-coated onto clean quartz coverslips and air-dried. The morphology of the dispersed film was checked with a scanning electron microscope. Material characterization was done with the following: Siemens D-500 X-ray diffractometer, JEOL 1200EX transmission electron microscope, and PerkinElmer UV/vis/NIR spectrophotometer with an integrating sphere, and a Spectralon reference. Micro-PL was measured using an Olympus IX70 microscope with an oil immersion 100× UV fluorescence objective (Immersol 518F and UPLSAPO, respectively). The excitation was a 350.7 nm line of a Kr ion laser. The power at the laser head was ~20 mW in most measurements, except for the experiments in Figure 3, where it was varied from 5 to 60 mW. Considering the losses in imaging beam transmission of the entire setup and the beam spot size, the power density at the sample is on the order of 10^6 to 10^7 mW/cm^2 (see Supporting Information, Figure S5). The emission filter was either a 385 nm long-pass, a 610 nm long-pass, or a 510 nm (teal) band-pass filter (Schott GG385, RG610, and BG-12, respectively), as noted in the text. The emission spectra were collected by an Acton SP2300i SpectraPro single monochromator and detected with a Spec-10 CCD camera. Imaging was done using an Andor Clara interline-CCD camera. Exposure times were 10 and 0.1 s per frame for the two cameras, respectively. Raman spectra were taken using the same microscope and objective with 10 mW, 413.1 nm excitation from a Kr ion laser passed through a holographic band-pass filter to remove plasma lines. A holographic notch filter following the sample was used to reject the scattered laser light. PL spectra of bulk samples were measured using the configuration described in ref 17, using a near-back-scattering geometry as shown in Figure S3 of Supporting Information. Bulk samples were intact films of TiO_2 nanotubes on Ti foil substrate or sintered films of 20 nm anatase nanoparticles (Aldrich) prepared as described in ref 19. Emission was recorded either in ambient air, in argon using 14 L/min flow of the gas, or in ethanol vapor as noted in the text. Dispersed films of conventional anatase TiO_2 nanoparticles (NPs) for micro-PL measurements were prepared starting from sintered films which were then sonicated and spin-coated onto quartz using the same procedure as described above for the nanotubes. For correlated SEM and micro-PL measurements, a grid was made by lithographic patterning with a positive resist and sputtering gold on quartz substrate (cleaned by acetone, isopropyl alcohol, and DI water and then air-dried).

Conflict of Interest: The authors declare no competing financial interest.

Acknowledgment. The support of the National Science Foundation through Grant CHE 0848511 is gratefully acknowledged. We thank Franceschi Microscopy and Imaging Center, Dr. Valerie Lynch-Holm and Riley Rex for the TEM images, Dr. Michael Rowe for XRD training, and Dr. Tom Dickinson and Dr. Enamul Khan for the diffuse reflectance measurement.

Supporting Information Available: TEM images, XRD, and diffuse reflectance spectra (Figure S1), power dependence of PL from a NP film (Figure S2), experimental configuration for measuring polarization dependence of NTA emission spectrum (Figure S3), epi-illumination, optical, and SEM images of dispersed NTs (Figure S4), determination of spot size and power density at the sample for 100× magnification (Figures S5 and S6). This material is available free of charge *via* the Internet at http://pubs.acs.org.

REFERENCES AND NOTES

1. O'Regan, B.; Gratzel, M. A Low-Cost, High-Efficiency Solar Cell Based on Dye-Sensitized Colloidal TiO_2 Films. *Nature* **1991**, *353*, 737–740.
2. Schwarzburg, K.; Willig, F. Influence of Trap Filling on Photocurrent Transients in Polycrystalline TiO_2. *Appl. Phys. Lett.* **1991**, *58*, 2520–2522.
3. De Jongh, P. E.; Vanmaekelbergh, D. Trap-Limited Electronic Transport in Assemblies of Nanometer-Size TiO_2 Particles. *Phys. Rev. Lett.* **1996**, *77*, 3427–3430.
4. Zhu, K.; Kopidakis, N.; Neale, N. R.; van de Lagemaat, J.; Frank, A. J. Influence of Surface Area on Charge Transport and Recombination in Dye-Sensitized TiO_2 Solar Cells. *J. Phys. Chem. B* **2006**, *110*, 25174–25180.
5. Benkstein, K. D.; Kopidakis, N.; van de Lagemaat, J.; Frank, A. J. Influence of the Percolation Network Geometry on Electron Transport in Dye-Sensitized Titanium Dioxide Solar Cells. *J. Phys. Chem. B* **2003**, *107*, 7759–7767.
6. Grimes, C. A. Synthesis and Application of Highly Ordered Arrays of TiO_2 Nanotubes. *J. Mater. Chem.* **2007**, *17*, 1451–1457.
7. Mohammadpour, R.; Irajizad, A.; Hagfeldt, A.; Boschloo, G. Comparison of Trap-State Distribution and Carrier Transport in Nanotubular and Nanoparticulate TiO_2 Electrodes for Dye-Sensitized Solar Cells. *Chem. Phys. Chem.* **2010**, *11*, 2140–2145.
8. Zhu, K.; Neale, N.; Miedaner, R. A.; Frank, A. J. Enhanced Charge-Collection Efficiencies and Light Scattering in Dye-Sensitized Solar Cells Using Oriented TiO_2 Nanotubes Arrays. *Nano Lett.* **2007**, *7*, 69–74.
9. Richter, C.; Schmuttenmaer, C. A. Exciton-like Trap States Limit Electron Mobility in TiO_2 Nanotubes. *Nat. Nanotechnol.* **2010**, *5*, 769–772.
10. Jennings, J. R.; Ghicov, A.; Peter, L. M.; Schmuki, P.; Walker, A. B. Dye-Sensitized Solar Cells Based on Oriented TiO_2 Nanotube Arrays: Transport, Trapping, and Transfer of Electrons. *J. Am. Chem. Soc.* **2008**, *130*, 13364–13372.

11. Cahen, D.; Hodes, G.; Grätzel, M.; Guillemoles, J. F.; Riess, I. Nature of Photovoltaic Action in Dye-Sensitized Solar Cells. *J. Phys. Chem. B* **2000**, *104*, 2053–2059.
12. Nelson, J. Continuous-Time Random-Walk Model of Electron Transport in Nanocrystalline TiO_2 Electrodes. *Phys. Rev. B* **1999**, *59*, 15374–15380.
13. Hendry, E.; Koeberg, M.; O'Regan, B.; Bonn, M. Local Field Effects on Electron Transport in Nanostructured TiO_2 Revealed by Terahertz Spectroscopy. *Nano Lett.* **2006**, *6*, 755–759.
14. Schwanitz, K.; Weiler, U.; Hunger, R.; Mayer, T.; Jaegermann, W. Synchrotron-Induced Photoelectron Spectroscopy of the Dye-Sensitized Nanocrystalline TiO_2/Electrolyte Interface: Band Gap States and Their Interaction with Dye and Solvent Molecules. *J. Phys. Chem. C* **2007**, *111*, 849–854.
15. Cass, M. J.; Qiu, F. L.; Walker, A. B.; Fisher, A. C.; Peter, L. M. Influence of Grain Morphology on Electron Transport in Dye Sensitized Nanocrystalline Solar Cells. *J. Phys. Chem. B* **2003**, *107*, 113–119.
16. Zhu, K.; Vinzant, T. B.; Neale, N. R.; Frank, A. J. Removing Structural Disorder from Oriented TiO_2 Nanotube Arrays: Reducing the Dimensionality of Transport and Recombination in Dye-Sensitized Solar Cells. *Nano Lett.* **2007**, *7*, 3739–3746.
17. Knorr, F. J.; Mercado, C. C.; McHale, J. L. Trap-State Distributions and Carrier Transport in Pure and Mixed-Phase TiO_2: Influence of Contacting Solvent and Interphasial Electron Transfer. *J. Phys. Chem. C* **2008**, *112*, 12786–12794.
18. Knorr, F. J.; Zhang, D.; McHale, J. L. Influence of $TiCl_4$ Treatment on Surface Defect Photoluminescence in Pure and Mixed-Phase Nanocrystalline TiO_2. *Langmuir* **2007**, *23*, 8686–8690.
19. Zhang, D.; Downing, J. A.; Knorr, F. J.; McHale, J. L. Room-Temperature Preparation of Nanocrystalline TiO_2 Films and the Influence of Surface Properties on Dye-Sensitized Solar Energy Conversion. *J. Phys. Chem. B* **2006**, *110*, 21890–21898.
20. Mercado, C. C.; Knorr, F. J.; McHale, J. L.; Usmani, S.; Ichimura, A.; Saraf, L. Location of Hole and Electron Traps on Nanocrystalline Anatase TiO_2. *J. Phys. Chem. C* **2012**, *116*, 10796–10804.
21. Diebold, U.; Ruzycki, N.; Herman, G. S.; Selloni, A. One Step towards Bridging the Materials Gap: Surface Studies of TiO_2 Anatase. *Catal. Today* **2003**, *85*, 93–100.
22. Mercado, C. C.; McHale, J. L. Defect Photoluminescence of TiO_2 Nanotubes. *Mater. Res. Soc. Symp. Proc.* **2009**, *1268*, EE0310.
23. Tachikawa, T.; Majima, T. Exploring the Spatial Distribution and Transport Behavior of Charge Carriers in a Single Titania Nanowire. *J. Am. Chem. Soc.* **2009**, *131*, 8485–8495.
24. Tachikawa, T.; Ishigaki, T.; Li, J. G.; Fujitsuka, M.; Majima, T. Defect-Mediated Photoluminescence Dynamics of Eu^{3+}-Doped TiO_2 Nanocrystals Revealed at the Single-Particle or Single-Aggregate Level. *Angew. Chem., Int. Ed.* **2008**, *47*, 5348–5352.
25. Jeon, K.-S.; Oh, S.-D.; Suh, Y. D.; Yoshikawa, H.; Masuhara, H.; Yoon, M. Blinking Photoluminescence Properties of Single TiO_2 Nanodiscs: Interfacial Electron Transfer Dynamics. *Phys. Chem. Chem. Phys.* **2009**, *11*, 534–542.
26. Mercado, C. C.; Seeley, Z.; Bandyopadhyay, A.; Bose, S.; McHale, J. L. Photoluminescence of Dense Nanocrystalline Titanium Dioxide Thin Films: Effect of Doping and Thickness and Relation to Gas Sensing. *ACS Appl. Mater. Interfaces* **2011**, *3*, 2281–2288.
27. Mor, G.; Varghese, O. K.; Paulose, M.; Shankar, K.; Grimes, C. A. A Review on Highly Ordered, Vertically Oriented TiO_2 Nanotube Arrays: Fabrication, Material Properties, and Solar Energy Applications. *Sol. Energy Mater. Sol. Cells* **2006**, *90*, 2011–2075.
28. Khairutdinov, R. F.; Burshtein, K. Ya.; Serpone, N. Photochemical Reactions on the Surface of a Circular Disk—A Theoretical Approach to Kinetics in Restricted Two-Dimensional Space. *J. Photochem. Photobiol. A* **1998**, *98*, 1–14.
29. Schmidt, T.; Lischka, K.; Zulehner, W. Excitation-Power Dependence of Near-Band-Edge Photoluminescence of Semiconductors. *Phys. Rev. B* **1992**, *45*, 8989–8994.
30. Enright, B.; Fitzmaurice, D. Spectroscopic Determination of Electron and Hole Effective Masses in a Nanocrystalline Semiconductor Film. *J. Phys. Chem.* **1996**, *100*, 1027–1035.
31. Johnson, J. C.; Yan, H.; Yang, P.; Saykally, R. J. Optical Cavity Effetcs in ZnO Nanowire Lasers and Waveguides. *J. Phys. Chem. B* **2003**, *107*, 8816–8828.
32. Tan, T.; Beydoun, D.; Amal, R. Effects of Organic Hole Scavengers on the Photocatalytic Reduction of Selenium Anions. *J. Photochem. Photobiol. A* **2003**, *159*, 273–280.
33. Hykaway, N.; Sears, W. M.; Morisaki, H.; Morrison, S. R. Current-Doubling Reactions on Titanium Dioxide Photoanodes. *J. Phys. Chem.* **1986**, *90*, 6663–6667.
34. Du, Y.; Deskins, N. A.; Zhang, Z.; Dohnalek, Z.; Dupuis, M.; Lyubinetsky, I. Formation of O Adatom Pairs and Charge Transfer upon O_2 Dissociation on Reduced TiO_2(110). *Phys. Chem. Chem. Phys.* **2010**, *12*, 6337–6344.
35. Deskins, N. A.; Dupuis, M. Intrinsic Hole Migration Rates in TiO_2 from Density Functional Theory. *J. Phys. Chem. C* **2009**, *113*, 346–358.
36. Nakade, S.; Saito, Y.; Kubo, W.; Kitamura, T.; Wada, Y.; Yanagida, S. Influence of TiO_2 Nanoparticle Size on Electron Diffusion and Recombination in Dye-Sensitized TiO_2 Solar Cells. *J. Phys. Chem. B* **2003**, *107*, 8607–8611.
37. Kamat, P. V.; Bedja, I.; Hotchandani, S. Photoinduced Charge Transfer between Carbon and Semiconductor Clusters: One-Electron Reduction of C_{60} in Colloidal TiO_2 Semiconductor Suspensions. *J. Phys. Chem.* **1994**, *98*, 9137–9142.
38. McHale, J. L.; Knorr, F. J. Photoluminescence and Carrier Transport in Nanocrystalline TiO_2. In *the Handbook of Luminescent Semiconductor Materials*; Bergman, L., McHale, J. L., Eds.; Taylor and Francis: Boca Raton, FL, 2012.
39. Macák, J. M.; Tsuchiya, H.; Schmuki, P. High-Aspect-Ratio TiO_2 Nanotubes by Anodization of Titanium. *Angew. Chem., Int. Ed.* **2005**, *44*, 2100–2102.